



Published in final edited form as:

Dev Cell. 2015 April 6; 33(1): 36–46. doi:10.1016/j.devcel.2015.02.012.

Systemic Organ Wasting Induced by Localized Expression of the Secreted Insulin/IGF Antagonist *ImpL2*

Young Kwon^{1,*}, Wei Song¹, Ilia A. Droujinine¹, Yanhui Hu¹, John M. Asara^{3,4}, and Norbert Perrimon^{1,2,*}

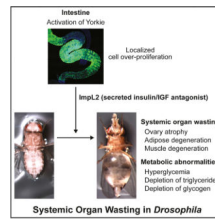
¹Department of Genetics, Harvard Medical School, Boston, MA 02115, USA

²Howard Hughes Medical Institute, Harvard Medical School, Boston, MA 02115, USA

³Department of Medicine, Harvard Medical School, Boston, MA 02115, USA

⁴Division of Signal Transduction, Beth Israel Deaconess Medical Center, Boston, MA 02115, USA

Abstract



SUMMARY

Organ wasting, related to changes in nutrition and metabolic activity of cells and tissues, is observed under conditions of starvation and in the context of diseases, including cancers. We have developed a model for organ wasting in adult *Drosophila*, whereby overproliferation induced by activation of Yorkie, the Yap1 oncogene ortholog, in intestinal stem cells leads to wasting of the ovary, fat body, and muscle. These organ-wasting phenotypes are associated with a reduction in systemic insulin/IGF signaling due to increased expression of the secreted insulin/IGF antagonist *ImpL2* from the overproliferating gut. Strikingly, expression of rate-limiting glycolytic enzymes and central components of the insulin/IGF pathway is upregulated with activation of Yorkie in the gut, which may provide a mechanism for this overproliferating tissue to evade the effect of *ImpL2*. Altogether, our study provides insights into the mechanisms underlying organ-wasting phenotypes in *Drosophila* and how overproliferating tissues adapt to global changes in metabolism.

© 2015 Elsevier Inc.

*Correspondence: ykwon@genetics.med.harvard.edu (Y.K.). perrimon@receptor.med.harvard.edu (N.P.).

ACCESSION NUMBERS

The accession number for the RNA-seq data reported in this paper is GEO: GSE65325.

SUPPLEMENTAL INFORMATION

Supplemental Information includes Supplemental Experimental Procedures, seven figures, and five tables and can be found with this article online at <http://dx.doi.org/10.1016/j.devcel.2015.02.012>.

INTRODUCTION

Wasting is the process characterized by an involuntary loss of body mass manifested in particular by degeneration of skeletal muscles and adipose tissues. Wasting is not only a physiological condition responding to extremely low energy intake and infection but also part of a complex systemic disorder associated with many diseases, including cancers, chronic obstructive lung disease, congestive heart failure, chronic kidney disease, and other chronic diseases (Deboer, 2009; Delano and Moldawer, 2006; Planté-Bordeneuve and Said, 2011; Tisdale, 1997). In particular, 50% of advanced cancer patients are affected by wasting syndrome, which accounts for approximately 20% of cancer death (Fearon et al., 2013; Penna et al., 2010). A number of studies have implicated proinflammatory cytokines, such as tumor necrosis factor α and interleukin 1 and 6, as secreted factors involved in wasting associated with various conditions (Fearon et al., 2013; Kir et al., 2014; Penna et al., 2010; Tisdale, 2009). Additionally, insulin-like growth factor 1 (IGF-1) signaling is a critical regulator of muscle mass maintenance (Bodine et al., 2001; Rommel et al., 2001; Sandri et al., 2004). Downregulation of IGF-1 signaling in skeletal muscles decreases Akt activity and in turn increases Foxo activity, which induces muscle protein degradation through the ubiquitin-proteasome system and autophagy (Han et al., 2013). Moreover, the transforming growth factor β family members myostatin and activin have been identified as additional secreted factors regulating organ wasting (Fearon et al., 2012; Han et al., 2013). Stimulation of myostatin/activin signaling in skeletal muscles activates Smad2/3 signaling and inhibits Akt signaling, which increases catabolism of muscle proteins (Fearon et al., 2012; Han et al., 2013).

The "bloating syndrome," observed in flies transplanted with imaginal discs mutant for the tumor suppressor *lethal (2) giant larvae (l(2)gl)* (Gateff and Schneiderman, 1974), is a systemic phenotype relevant to the wasting syndrome. Whereas a wild-type imaginal disc transplanted into the abdomen of an adult fly only grows until it reaches its normal size, a transplanted *l(2)gl* mutant disc undergoes neoplastic growth and eventually kills the fly. However, before they die, these flies develop the bloating syndrome, whereby the abdomen becomes swollen and translucent and the fat body and ovaries are almost completely degenerated (Gateff and Schneiderman, 1974). This degeneration of the fat body and ovaries is reminiscent of the wasting of adipose tissue and skeletal muscles in mammals, because the fat body and ovaries are the organs preserving energy in the forms of lipids and proteins in *Drosophila*. Strikingly, although the bloating syndrome is a robust phenotype, it has not been characterized in detail. In particular, it is not known whether the wasting process affects metabolism and how neoplastic *l(2)gl* mutant discs induce degeneration of ovaries and the fat body.

The transcriptional coactivator *yorkie (yki)* regulates growth, repair, and regeneration by inducing a transcriptional program required for cell proliferation and survival (Halder and Johnson, 2011; Harvey and Hariharan, 2012; Pan, 2010; Staley and Irvine, 2012; Yang and Xu, 2011). In particular, studies in adult *Drosophila* have identified a crucial role of *yki* in the regulation of intestinal stem cell (ISC) proliferation during tissue homeostasis and damage (Karpowicz et al., 2010; Ren et al., 2010; Shaw et al., 2010). Furthermore, these studies have shown that activation of Yki in the midgut induces massive cell proliferation,

which conceivably affects the physiology of the proliferating tissue as well as the homeostasis of distant tissues and the whole organism. However, it is not known whether and how localized cell proliferation in the midgut driven by activation of Yki perturbs the physiology and function of distant organs and the whole organism.

Here we show that induction of aberrant cell proliferation in the midgut by activation of Yki causes the bloating syndrome, which is associated with degeneration of the ovary, fat body, and muscle. We characterize in detail the systemic wasting phenotypes associated with the proliferating midgut using genomic, metabolomic, and physiological analyses. Finally, we show that the secreted insulin/IGF antagonist *ImpL2* is involved in the wasting process by decreasing systemic insulin/IGF signaling.

RESULTS

Localized Aberrant Cell Proliferation Induced by Activation of Yki in ISCs Causes Systemic Organ Wasting

To address how localized aberrant cell proliferation alters organismal homeostasis, we expressed an active form of *yki* (*yki^{act}*) (Oh and Irvine, 2009) in adult midgut ISCs using the conditional GAL4 driver *esg^{ts}* (*esg-GAL4, tub-GAL80^{ts}, UAS-GFP/+*) (hereafter referred to as *esg^{ts}>yki^{act}*). Consistent with the proposed role of *yki* in the midgut (Karpowicz et al., 2010; Ren et al., 2010; Shaw et al., 2010), expression of *yki^{act}* resulted in massive cell proliferation as detected by an increase in GFP signal and aberrant shape of the gut (Figure 1A). Strikingly, over time, these flies developed the bloating syndrome phenotype (Figures 1B and B'), originally described in adult flies with transplanted imaginal discs harboring a mutation in the tumor suppressor *l(2)gl* in the abdomen (Gateff and Schneiderman, 1974). *esg^{ts}>yki^{act}* flies exhibit this bloating phenotype as early as 5 days after induction of *yki^{act}*. Both the penetrance and severity of the phenotype progressively increase, with ~70% of flies showing the phenotype at 6 days (Figure 1B) and ~95% at 12 days (Figure 1B'). Additionally, ovaries and fat bodies of *esg^{ts}>yki^{act}* females degenerate progressively with time (Figures 1C and 1D). In adult flies, the fat body does not form as a discrete structure but fills the abdominal space, resulting in a continuous light yellow mass. Whereas fat bodies in controls were not affected (Figures 1B and 1D), the fat bodies in *esg^{ts}>yki^{act}* flies were observed as discontinuous patches at 6 days (Figures 1B and 1D') and were almost completely degenerated at 12 days of *yki^{act}* induction (Figure 1B'; magnified images are not shown). Furthermore, we observed accelerated decline of muscle function in *esg^{ts}>yki^{act}* flies. *esg^{ts}>yki^{act}* flies showed progressive climbing defects (Figure 1E) and downturned wings (Figure 1F), general indicators of muscle weakening/degeneration (Demontis and Perrimon, 2010; Greene et al., 2003). To characterize the underlying cellular defects associated with muscle weakening/degeneration in *esg^{ts}>yki^{act}*, we examined the structures of *esg^{ts}>yki^{act}* muscles by electron microscopy. Mitochondria of *esg^{ts}>yki^{act}* muscles were swollen and often associated with empty space (Figure 1G). Moreover, cristae were fragmented, and inner mitochondrial space was filled with low-electron-dense sectors (Figure 1G'), indicative of mitochondrial degeneration (Greene et al., 2003). Altogether, these findings reveal that aberrant cell proliferation induced by activation of Yki in ISCs causes systemic organ-wasting phenotypes affecting ovaries, fat body, and muscle.

Expression of *yki^{act}* in Midgut Causes Repression of Genes Involved in Energy Metabolism in Muscle

To gain insight into the systemic phenotypes induced by *esg^{ts}>yki^{act}*, we performed a transcriptomic analysis of thoracic muscles (Table S1), which play an important role in the regulation of organismal physiology and aging by affecting systemic insulin/IGF signaling and trehalose/glucose metabolism (Demontis and Penimon, 2010). Interestingly, gene list enrichment analysis of the downregulated muscle transcriptome revealed a striking enrichment of multiple metabolic processes impinging on carbohydrate metabolism ($p = 0.0018$), amino acid metabolism ($p = 1.32 \times 10^{-7}$), metabolism of vitamins and cofactors ($p = 1.32 \times 10^{-7}$), and metabolism of xenobiotics by cytochrome P450 ($p = 1.45 \times 10^{-4}$) (Figure 2A; Tables S2 and S3). Furthermore, we found a systematic repression of genes involved in energy metabolism ($p = 0.000$, gene set enrichment analysis; GSEA), including glycolysis ($p = 0.018$, GSEA), pyruvate metabolism and the citric acid cycle ($p = 0.0252$, GSEA), and oxidative phosphorylation ($p = 0.000$, GSEA) (Figures 2A and 2B; Figure S1; Table S4). We further confirmed by quantitative (q)PCR that the expression of multiple genes involved in glycolysis was decreased not only in muscles but also in ovaries of *esg^{ts}>yki^{act}* flies (Figures 2C and 2D). Moreover, the activities of the two rate-limiting glycolytic enzymes Hexokinase (Hex-A and Hex-C) and Phosphofructokinase (Pfk) are reduced by approximately 30% in *esg^{ts}>yki^{act}* muscle (Figure 2E). Accordingly, ATP levels in muscles were significantly decreased in *esg^{ts}>yki^{act}* flies as compared to controls (Figure 2F). Moreover, metabolomic analyses revealed a decrease of ATP, NADH, and NADPH levels in the hemolymph of *esg^{ts}>yki^{act}* flies (Figure 2G; Figure S2; Table S5), which are the main products of energy metabolism. Altogether, these results suggest that *esg^{ts}>yki^{act}* alters the metabolic gene expression program of distant tissues, which is manifested by downregulation of genes involved in glycolysis in muscle and ovaries.

Overproliferating Midgut due to Activation of Yki Causes Hyperglycemia

Because we observed that gene expression of glycolytic enzymes in muscles and ovaries was downregulated in *esg^{ts}>yki^{act}* flies, we investigated whether there were any changes in glucose metabolism in these flies. As expected from the bloating phenotype, the volume of extractable hemolymph from *esg^{ts}>yki^{act}* flies was greatly increased as compared to controls (Figure 3A). Nevertheless, the concentration of trehalose, the primary circulating sugar composed of two alpha-glucoses, was significantly increased in the hemolymph of *esg^{ts}>yki^{act}* flies (Figure 3B). Accordingly, whole-body trehalose levels were increased in *esg^{ts}>yki^{act}* flies (Figure 3C). Additionally, consistent with the degeneration of the fat body that stores triglycerides and glycogen in the adult, whole-body triglycerides and glycogen levels were reduced in *esg^{ts}>yki^{act}* flies, as compared to controls (Figures 3D and 3E).

Starvation causes a reduction in whole-body trehalose levels (Figure S3B), suggesting that the increase of trehalose levels in *esg^{ts}>yki^{act}* flies is not due to the effect of starvation (Figures 3B and 3C). Nevertheless, starvation affects storage of triglycerides and glycogen (Figures S3C and S3D). Thus, because the presence of cell overproliferation in the midgut could in principle perturb gut functions and mimic starvation, we addressed whether *esg^{ts}>yki^{act}* altered food intake and absorption. Measurements of food intake and excretion did not appear to be significantly affected in *esg^{ts}>yki^{act}* flies (Figures 3F and 3G). To

further test whether *esg^{ts}>yki^{act}* flies are starved, we examined *Drosophila* insulin-like peptide 2 (Dilp2) levels in Dilp-producing cells (QPCs) in the brain, because starvation causes accumulation of *Dilp2*, presumably due to a reduction in secretion (Demontis and Perrimon, 2010; Géminard et al., 2009; Ikeya et al., 2002). Surprisingly, the Dilp2 signal in the IPCs of *esg^{ts}>yki^{act}* flies was significantly decreased (Figures 3H and 3I). This decrease of Dilp2 signal is not due to a reduction in *Dilp2* mRNA, as we observed that the levels of *Dilp* mRNAs in the heads remained unaffected in *esg^{ts}>yki^{act}* flies (Figure 3J). Moreover, we tested a starvation marker, *Pepck*, which is regulated by both sugar and glycine (Zinke et al., 1999), and found that *Pepck* mRNA expression was increased so-fold during starvation (Figure S3F). Conversely, *Pepck* mRNA expression remained unaltered at 6 days of *yki^{act}* induction and increased ~3-fold at 12 days (Figure S3F), suggesting that *esg^{ts}>yki^{act}* flies were not severely starved. Altogether, these findings indicate that aberrant cell proliferation, induced by activation of *yki*, causes systemic abnormality in trehalose/glucose metabolism, which resembles hyperglycemia. Further, because Dilp2 is not accumulated in the IPCs and *Pepck* expression is not greatly affected, it is unlikely that starvation is the main cause of the phenotypes associated with *esg^{ts}>yki^{act}*. However, we cannot rule out that other aspects of gut function are perturbed, contributing to the organ-wasting and bloating phenotypes (see Discussion).

Depletion of *ImpL2* from *esg^{ts}>yki^{act}* Midguts Rescues Systemic Reduction of Akt1 Phosphorylation and Hyperglycemia

To identify the signaling factor(s) impinging on systemic phenotypes in *esg^{ts}>yki^{act}* flies, we interrogated the muscle transcriptome of *esg^{ts}>yki^{act}*. Interestingly, target genes of Foxo, a transcription factor inhibited by insulin/IGF signaling, are enriched in the upregulated muscle transcriptome of *esg^{ts}>yki^{act}* flies ($p = 0.039$; Figure 4A). In particular, *Thor* (human 4E-BP ortholog), a well-characterized target of Foxo, is significantly upregulated (Figure 4B). Consistent with the transcriptome analysis results, Akt phosphorylation is significantly reduced in muscles and heads of *esg^{ts}>yki^{act}* flies (Figure 4C). To characterize the mechanism by which *esg^{ts}>yki^{act}* reduces systemic insulin/IGF signaling, we examined whether the expression of *ImpL2*, a secreted protein that resembles IGFBP7 (Sloth Andersen et al., 2000) and that inhibits insulin/IGF signaling by forming a protein complex with circulating Oilps (Alic et al., 2011; Honegger et al., 2008), was affected in *esg^{ts}>yki^{act}* flies. Strikingly, *ImpL2* mRNA expression was greatly elevated in *esg^{ts}>yki^{act}* midguts at 6 days of *yki^{act}* induction, whereas the expression of *ImpL2* remained unchanged in muscles, ovaries, heads, and fat bodies (Figure 4D). Interestingly, starvation regulates *ImpL2* expression (Honegger et al., 2008), and we further confirmed that starvation increased *ImpL2* mRNA expression in heads, muscles, midguts, and fat bodies (Figure S3E). The absence of *ImpL2* mRNA induction in the muscles, ovaries, heads, and fat bodies of *esg^{ts}>yki^{act}* flies further supports that these flies are not calorie deprived. Moreover, *ImpL2* mRNA expression is increased ~70-fold in the *esg^{ts}>yki^{act}* midgut, which appears to greatly exceed the range of induction during starvation (Figure 4D; Figure S3E).

To address the role of *ImpL2*, we examined whether removal of *ImpL2* activity could rescue the systemic phenotypes associated with *esg^{ts}>yki^{act}*. The null allele *ImpL2^{Def20}* (Honegger et al., 2008) completely rescued the reduction of Akt1 phosphorylation in *esg^{ts}>yki^{act}* flies

(Figure 4C) and restored circulating trehalose concentration and whole-body trehalose levels (Figures S4A and S4B). The rescue of the systemic phenotypes associated with *esg^{ts}>yki^{act}* by *ImpL2^{Def20}* is presumably due to a systemic increase of insulin/IGF signaling, as *ImpL2^{Def20}* alone caused a slight increase of Akt1 phosphorylation (Figure 4C) and reduction of circulating trehalose concentration (Figure S4A). Next, to examine the importance of *ImpL2* induction in the midgut, we coexpressed an RNAi against *ImpL2* (*15009R-3*) together with *yki^{act}*. The expression of *ImpL2*-RNAi efficiently suppressed the induction of *ImpL2* in *esg^{ts}>yki^{act}* midgut (~80% knockdown efficiency), although the expression of *ImpL2* remained 8-fold higher than in controls (Figure S4C). Notably, expression of *ImpL2*-RNAi alone using *esg^{ts}* did not significantly alter Akt1 phosphorylation and trehalose levels (Figures 4C, 4E, and 4F). Importantly, knockdown of *ImpL2* with *esg^{ts}* restored Akt1 phosphorylation in muscles and heads significantly (Figure 4C) and reduced the trehalose levels (Figures 4E and 4F). This rescue is not due to suppression of cell proliferation, because the overall shape and GFP intensity of *esg^{ts}>yki^{act}* midguts remained unaltered after *ImpL2*-RNAi expression (Figure 4G). Additionally, similar experiments employing an additional *ImpL2*-RNAi line (*30931*) further confirmed the importance of *ImpL2* induction in the midgut for the systemic phenotypes associated with *esg^{ts}>yki^{act}* (Figures S4O–S4F). In addition, ectopic expression of *ImpL2* in enterocytes (ECs) in the midgut caused hyperglycemia, reduction of Akt1 phosphorylation in muscle, increase of hemolymph volume, and ovary atrophy (Figures S4G–S4K), suggesting that the increased *ImpL2* expression was sufficient to cause some of the systemic phenotypes associated with *esg^{ts}>yki^{act}*. Altogether, our results indicate that induction of *ImpL2* in *esg^{ts}>yki^{act}* midguts is a critical determinant for both the hyperglycemia and systemic reduction of insulin/IGF signaling in *esg^{ts}>yki^{act}* flies.

Depletion of *ImpL2* in *esg^{ts}>yki^{act}* Midguts Rescues Ovary Wasting and Muscle Degeneration

Next, we addressed whether *ImpL2* is involved in the organ-wasting process associated with *esg^{ts}>yki^{act}*. Interestingly, either *ImpL2^{def20}* or depletion of *ImpL2* in the midgut with *esg^{ts}* suppressed wasting of ovaries caused by *esg^{ts}>yki^{act}* (Figure SA). In addition, expression of *ImpL2* in the midgut is required for the muscle degeneration observed in *esg^{ts}>yki^{act}* flies. Depletion of *ImpL2* in the midgut with *esg^{ts}* rescued the climbing defects and downturned wings in *esg^{ts}>yki^{act}* flies (Figures 1E, 1F, 5B, and 5C). Strikingly, expression of *ImpL2*-RNAi with *esg^{ts}* was sufficient to significantly rescue the mitochondrial defects (Figures 1G, 1G', SD, and SD') and reduced ATP levels (Figures 2F and 5E). Finally, we found that the bloating phenotype in *esg^{ts}>yki^{act}* flies was also dependent on *ImpL2*, because knockdown of *ImpL2* in the midgut with *esg^{ts}* significantly rescued the bloating phenotype (Figure 5F). Altogether, these results indicate that degeneration of ovaries and muscle in *esg^{ts}>yki^{act}* flies is dependent on increased expression of *ImpL2* in the midgut.

Expression of Insulin/IGF Pathway Components and Glycolytic Enzymes Is Upregulated in the Proliferating Midgut due to Aberrant Activation of Yki

Although insulin/IGF signaling is indispensable for *yki^{act}*-mediated cell proliferation in the midgut (data not shown), *esg^{ts}>yki^{act}* midguts undergo cell proliferation irrespective of the

induction of *ImpL2*. Strikingly, instead of observing a reduction of Akt1 phosphorylation, expression of *yki^{act}* increased the levels of both pAkt1 and Akt1 in the midgut (Figures 6A and 6B), similar to a previous observation in the wing disc (Ye et al., 2012). Moreover, overall Akt1 phosphorylation in the midgut was greatly increased as compared to control (Figure S5). Interestingly, we found that gene expression of insulin/IGF pathway components was systematically increased in *esg^{ts}>yki^{act}* midgut (*InR*, ~8-fold; *Akt1*, ~12-fold; Figure 6C). Conversely, the mRNA levels of these genes were not affected significantly in muscles and ovaries, with the exception of *InR* in muscles (Figure S6). Finally, expression of *yki^{act}* in the midgut elevated the transcript of *Dilp3*, which regulates insulin/IGF signaling in that tissue (O'Brien et al., 2011) (Figure 6D). Thus, our findings suggest that expression of *yki^{act}* in the midgut causes a disparity in the activity of insulin/IGF signaling between the midgut and other tissues. Interestingly, extracellular signal-regulated kinase activation was shown to enhance insulin/IGF signaling by increasing the expression of *InR* transcript (Zhang et al., 2011). Additionally, *ras^{V12}; csk^{-/-}* transformed cells increased *InR* expression through Wingleless signaling to evade the insulin resistance induced by a high-sugar diet (Hirabayashi et al., 2013). Although Foxo is a well-characterized transcription factor regulating *InR* expression (Puig and Tjian, 2005), these observations and ours suggest that some mitogenic signals can enhance insulin/IGF signaling by increasing *InR* expression.

This disparity of insulin/IGF signaling activities presumably leads to differential regulation of glucose metabolism between the midgut and other tissues. In contrast to the observations in muscles and ovaries (Figures 2C and 2D), the mRNA expression of glycolytic enzymes was systematically increased in *esg^{ts}>yki^{act}* midguts (Figure 6E). In particular, the mRNA levels of two key rate-limiting enzymes, *Hex-A* and *Pfk*, were increased by ~4- and ~10-fold, respectively, and the ortholog of lactate dehydrogenase, *ImpL3*, which is a major contributor to the Warburg effect (Vander Heiden et al., 2009; Warburg, 1956), was increased ~7-fold. Consistent with overproliferation in the midgut, we observed increased glucose incorporation in *esg^{ts}>yki^{act}* midgut as compared to controls (Figure 6F). Strikingly, in other parts of these flies, glucose incorporation was reduced by ~50% (Figure 6F), a process dependent on wild-type *ImpL2* allele, because *ImpL2^{def20}* rescued the reduction of glucose incorporation in the whole-body void of midgut and hemolymph induced by *esg^{ts}>yki^{act}* (Figure 6F). Altogether, these observations suggest that activation of *yki* in the midgut causes a bias in glucose metabolism between the midgut and other tissues, and that *ImpL2* is a genetic determinant of this phenomenon.

DISCUSSION

In this study, we describe the unexpected observation that the overproliferating midgut due to aberrant Yki activity in ISCs induces the bloating syndrome and systemic organ wasting. Additionally, the overproliferating midgut perturbs organismal metabolism, resulting in an increase of hemolymph trehalose and depletion of glycogen and triglyceride storage (Figure 7). Strikingly, we show that the accumulation of hemolymph trehalose and organ-wasting processes are dependent on the antagonist of insulin/IGF signaling, *ImpL2*, which is specifically upregulated in the proliferating midgut. Our study provides strong genetic evidence supporting that systemic organ wasting associated with the aberrant activation of

Yki in ISCs cannot be explained solely by the perturbation of general gut function. Based on these findings, we propose that *ImpL2* is a critical factor involved in systemic organ wasting in *Drosophila*.

In an accompanying paper in this issue of *Developmental Cell*, Figueroa-Clarevega and Bilder show that transplantation of *scrib¹/Ras^{VI2}* disc tumors into wild-type flies induces the bloating syndrome phenotype and systemic organ wasting, affecting ovaries, fat bodies, and muscles (Figueroa-Clarevega and Bilder, 2015). Figueroa-Clarevega and Bilder also identify *ImpL2* as a tumor-driven factor that plays a critical role in the organ-wasting process. These results are consistent with our findings and indicate that the bloating syndrome and organ-wasting phenotypes are not associated specifically with perturbation of gut function. Interestingly, Figueroa-Clarevega and Bilder observe that disc tumors derived by the expression of *yki^{S/A}* (an active form of *yki* that is less potent than *yki^{act}* used in this study) did not cause organ wasting, which can be explained by the low level of *ImpL2* induction in the *yki^{S/A}* tumors as compared to *scrib¹/Ras^{VI2}* tumors.

Our results do not rule out the existence of an additional factor(s) contributing to the bloating syndrome and organ-wasting phenotypes. Indeed, the partial rescue of the bloating syndrome and organ-wasting phenotypes by depletion of *ImpL2* in *esg^{ts}>yki^{act}* midguts suggests the existence of an additional factor(s). Moreover, we observed that ectopic expression of *ImpL2* in ECs was not sufficient to reduce whole-body triglyceride and glycogen levels (data not shown), although it caused hyperglycemia, reduction of Akt1 phosphorylation, and increase of hemolymph volume (Figures S4G-S4J). Thus, given the involvement of diverse factors in the wasting process in mammals, it is likely that in addition to *ImpL2*, another factor(s) contributes to systemic organ wasting in *Drosophila*.

Our study shows that the bloating syndrome caused by *esg^{ts}>yki^{act}* is associated with *ImpL2*, as depletion of *ImpL2* from *esg^{ts}>yki^{act}* midguts significantly rescues the bloating phenotype. Given the observation that elevated expression of *ImpL2* from *esg^{ts}>yki^{act}* midgut induces hyperglycemia, we speculate that the accumulation of trehalose in hemolymph is a factor involved in bloating, because a high concentration of trehalose can cause water influx to adjust hemolymph osmolarity to physiological levels. Interestingly, recent findings have shown that disruption of *l(2)gl* in discs activates *yki* (Grzeschik et al., 2010; Halder and Johnson, 2011; Menéndez et al., 2010; Staley and Irvine, 2012), suggesting that the bloating syndrome observed in flies with transplanted *l(2)gl* mutant discs may be due to aberrant *yki* activity.

Our findings are reminiscent of a previous study showing that in *Drosophila*, humoral infection with the bacterial pathogen *Mycobacterium marinum*, which is closely related to *Mycobacterium tuberculosis*, causes a progressive loss of energy stores in the form of fat and glycogen—a wasting-like phenotype (Dionne et al., 2006). Similar to our observation, Dionne et al. found that infection with *M. marinum* caused a downregulation of Akt1 phosphorylation. Given our observation that *ImpL2* produced from *esg^{ts}>yki^{act}* affects systemic insulin/IGF signaling, it will be of interest to test whether *ImpL2* expression is increased upon infection with *M. marinum* and mediates the effect on the loss of fat and glycogen storage.

yki plays critical roles in tissue growth, repair, and regeneration by inducing cell proliferation (Johnson and Halder, 2014; Pan, 2010; Staley and Irvine, 2012), a process requiring additional nutrients to support rapid synthesis of macromolecules including lipids, proteins, and nucleotides. In particular, increased aerobic glycolysis metabolizing glucose into lactate is a characteristic feature of many cancerous and normal proliferating cells (Vander Heiden et al., 2011). Interestingly, the aberrant activation of *yki* in ISCs caused a disparity in the gene expression of glycolytic enzymes and the activity of insulin/IGF signaling between the proliferating midgut and other tissues, such as muscle and ovaries (Figure 7). Thus, we speculate that this disparity favors Yki-induced cell proliferation by increasing the availability of trehalose/glucose to the proliferating midgut, which presumably requires high levels of trehalose/glucose (Figure 7). Additionally, it will be of interest to test whether activation of Yki during tissue growth, repair, and regeneration alters systemic metabolism in a similar manner.

EXPERIMENTAL PROCEDURES

Fly Stocks and Manipulation of Midgut Progenitor Cells

UAS-yki^{act} (*w**; *UAS-yki.S111A.S168A.S250A.V5*; 228817) (Oh and Irvine, 2009) was obtained from the Bloomington *Drosophila* Stock Center. *esg^{ts}* refers to *tub-GAL80^{ts}*, *esg-GAL4*, *UAS-GFP* (II) (Apidianakis et al., 2009). RNAi line *15009R-3* against *ImpL2* was obtained from the National Institute of Genetics, Japan. *30931* is an RNAi line against *ImpL2* obtained from the Vienna *Drosophila* Resource Center, Austria. RNAi lines obtained from the Transgenic RNAi Project (<http://www.flyrnai.org>) are *JF01482* (*InR*), *JF01987* (*Pten*), and *HM04007* (*Akt1*). Additionally, we used *UAS-Pten* (III), *UAS-myr-Akt1* (III), and *ImpL2^{Def20}* (gift from Hugo Stocker).

To induce transgenes in midgut stem cells, we followed the experimental procedures described previously (Apidianakis et al., 2009). Briefly, crosses were set up with *esg^{ts}* at room temperature, and after 3 days of incubation at room temperature were transferred to 18°C to activate GAL80^{ts} thus restricting the expression of the Gal4 induced transgenes. Zero- to 4-day-old adult progenies were collected and placed at 29°C to induce the transgenes. Progenies from a cross between *esg^{ts}* and *w¹¹¹⁸* were used as controls. During incubation at 29°C, flies were transferred onto fresh food every 2 days.

Measurement of Carbohydrate and Triglyceride Levels

We measured fly carbohydrates and triglycerides as described previously (Song et al., 2010, 2014; Teleman et al., 2005). To prepare fly lysates for metabolic assays, we homogenized six female adults from each group in 400 µl PBS supplemented with 0.2% Triton X-100, heated the homogenate at 70°C for 5 min, and collected the supernatant after centrifugation at 14,000 rpm for 10 min. Whole-body trehalose levels were measured from 10 µl of supernatant treated with 0.2 µl trehalase (Megazyme; E-TREH) at 37°C for 30 min using glucose assay reagent (Megazyme; K-GLUC) following the manufacturer's protocol. We subtracted the amount of free glucose from the measurement and then normalized the subtracted values to protein levels in the supernatant. Whole-body glycogen levels were determined from 10 µl of supernatant preincubated with 1 µl amyloglucosidase (Sigma-

Aldrich; A7420) at 37°C for 30 min using glucose assay reagent (Megazyme; K-GLUC). Free glucose levels were subtracted from the measurements, and glycogen levels were normalized to total protein levels. To measure whole-body triglycerides, we processed 10 µl of supernatant using a Serum Triglyceride Determination kit (Sigma-Aldrich; TR0100). We subtracted the amount of free glycerol in the supernatant from the measurement and then normalized the subtracted values to protein levels in the supernatant.

To measure circulating trehalose concentrations, hemolymph was extracted from 10–20 decapitated female adults by centrifugation at $1,500 \times g$ for 15 min. Half a microliter of the collected hemolymph was diluted in 40 µl of TBS buffer (5 mM Tris-HCl [pH 6.6], 137 mM NaCl, 2.7 mM KCl), heated at 70°C for 5 min, and centrifuged at 14,000 rpm for 10 min. The supernatant was treated with 02 µl trehalase (Megazyme; E-TREH) at 37°C for 30 min and then used to measure circulating trehalose levels with glucose assay reagent (Megazyme; K-GLUC). We subtracted the amount of free glucose in the supernatant from the measurement.

Hemolymph volumes were measured using either a micropipette P2.5 (Eppendorf) or P10 (Gilson) and normalized to the number of flies used for hemolymph extraction.

Glucose Incorporation Assay

Fifteen to 25 flies incubated at 29°C for 3 days were transferred onto fresh food with 2 µCi [U-¹⁴C]glucose (PerkinElmer; NEC042V). After 2 days of incubation at 29°C, the flies were transferred again onto fresh food with 2 µCi [U-¹⁴C] glucose and incubated for an additional 2 days. To remove the food in the gut, we placed the flies onto nonradioactive food for 7–8 hr prior to dissection. Then, seven midguts were dissected in PBS and collected in 250 µl RIPA buffer (50 mM Tris-HCl [pH 7.4], 150 mM NaCl, 1% sodium deoxycholate, 1 mM EDTA, 0.1% SDS, 1% NP-40) after rinsing them twice with PBS. To collect the whole-body void of midgut and hemolymph, we dissected out the midguts through a small incision in the abdomen. Dissected flies were placed in an Eppendorf tube with 1 ml PBS and then washed four times with 1 ml PBS by inverting three to five times. Three dissected flies were homogenized in 250 µl RIPA buffer. After homogenization, we added 300 µl water to the homogenates to increase the volume. Five hundred microliters of homogenate was mixed with 10 ml Ultima Gold liquid scintillation cocktail (PerkinElmer; 6013326) in 20-ml glass scintillation vials. Disintegrations per minute values were measured and normalized to control.

RNA Sequencing Analysis of Muscle Transcriptome

To extract total RNAs for RNA sequencing (RNA-seq) experiments, we used ten thoraces dissected out from flies incubated for 8 days at 29°C. After assessing RNA quality with an Agilent Bioanalyzer, mRNAs were enriched by poly(A) pull-down. Then, sequencing libraries constructed with an Illumina TruSeq RNA preparation kit were sequenced using an Illumina HiSeq 2000 at the Columbia Genome Center (<http://systemsbiology.columbia.edu/genome-center>). We multiplexed samples in each lane, which yields a targeted number of single-end 100-bp reads for each sample, as a fraction of 180 million reads for the whole lane. Sequence reads were mapped back to the *Drosophila* genome (FlyBase genome

annotation version r5.51) using TopHat (Trapnell et al., 2009). With the uniquely mapped reads, we quantified gene expression levels using Cufflinks (Trapnell et al., 2012) (reads per kb of exon per million fragments mapped values). Next, we performed data normalization on the read counts and applied a negative binomial statistical framework using the Bioconductor package DESeq to quantify differential expression between experimental and control data. The RNA-seq data were deposited in the Gene Expression Omnibus (accession number GSE65325).

Metabolomics of Hemolymph Metabolites

To collect hemolymph, thoraces of approximately 200 flies were pierced with a tungsten needle. Next, the flies were placed in a perforated 0.5-ml Eppendorf tube within a 1.5-ml Eppendorf tube and then centrifuged twice at $2,348 \times g$ for 4 min at 4°C with a gentle mixing of the flies between centrifugations. Collected hemolymph was centrifuged again at $2,348 \times g$ for 3 min to precipitate hemocytes and other debris. The supernatant was centrifuged at $14,000 \times g$ for 15 min to remove the insoluble fraction. Processed hemolymph was flash-frozen on dry ice and kept at -80°C until metabolomic sample preparation.

Metabolomic samples were prepared essentially as described previously (Yuan et al., 2012). Briefly, a hemolymph sample was diluted in -80°C methanol for a final methanol concentration of 80%. Then, the sample was briefly vortexed and stored at -80°C overnight. The sample was then centrifuged at $14,000 \times g$ for 10 min. The supernatant was dried in a SpeedVac and then frozen at -80°C . For liquid chromatography tandem mass spectrometry (LC-MS/MS), the resuspended sample in 20 μl of LC-MS-grade water was centrifuged and 10 μl was injected. Mass spectrometry was performed as described previously (Yuan et al., 2012) at the Beth Israel Deaconess Medical Center Mass Spectrometry Facility (<http://www.bidmcmassspec.org>). Briefly, selected reaction monitoring of 287 Q1/Q3 transitions was targeted in positive/negative switching mode using a SSOO QTRAP hybrid triple quadrupole mass spectrometer (AB SCIEX). Amide HPLC chromatography (Waters) was used at high pH over a 20-min gradient. Integrated peak area values of each metabolite were normalized to hemolymph volume or fly number.

Supplementary Material

Refer to Web version on PubMed Central for supplementary material.

ACKNOWLEDGMENTS

We thank the Transgenic RNAi Project, National Institute of Genetics (Japan), and Bloomington *Drosophila* Stock Center for fly stocks, Dr. Hugo Stocker for *ImpL2* stocks, and Drs. Stephanie Mohr, Richelle Sopko, Jonathan Zirin, Richard Binari, and Akhila Rajan for comments on the manuscript. We thank Alejandra Figueroa-Clavega and David Bilder for exchange of information on the role of *ImpL2* before publication. We also thank Min Yuan for help with the mass spectrometry experiments. Y.K. was supported in part by the Damon Runyon Cancer Research Foundation. This work was supported in part by P01 CA120964 (J.M.A. and N.P.) and R01 DK088718 (N.P.). N.P. is an Investigator of the Howard Hughes Medical Institute.

REFERENCES

- Alic N, Hoddinott MP, Vinti G, Partridge L. Lifespan extension by increased expression of the *Drosophila* homologue of the IGFBP7 tumour suppressor. *Aging Cell*. 2011; 70:137–147. [PubMed: 21108726]
- Apidianakis Y, Pitsouli C, Perrimon N, Rahme L. Synergy between bacterial infection and genetic predisposition in intestinal dysplasia. *Proc. Natl. Ac ad. Sci. USA*. 2009; 106:20883–20888.
- Benjamini Y, Hochberg Y. Controlling the false discovery rate: a practical and powerful approach to multiple testing. *J. R. Stat. Soc. Series B Stat. Methodol*. 1995; 57:289–300.
- Bodine SC, Stitt TN, Gonzalez M, Kline WO, Stover GL, Bauerlein R, Zlotchenko E, Scrimgeour A, Lawrence JC, Glass DJ, Yancopoulos GD. Akt/mTOR pathway is a crucial regulator of skeletal muscle hyper trophy and can prevent muscle atrophy invivo. *Nat. Cell Biol*. 2001; 3:1014–1019. [PubMed: 11715023]
- Deboer MD. Animal models of anorexia and cachexia. *Expert Opin. Drug Discov*. 2009; 4:1145–1155. [PubMed: 20160874]
- Delano MJ, Moldawer LL. The origins of cachexia in acute and chronic inflammatory diseases. *Nutr. Clin. Pract*. 2006; 21:68–81. [PubMed: 16439772]
- Demontis F, Perrimon N. FOXO/4E-BP signaling in *Drosophila* muscles regulates organism-wide proteostasis during aging. *Cell*. 2010; 143:813–825. [PubMed: 21111239]
- Dionne MS, Pham LN, Shirasu-Hiza M, Schneider DS. Aki and FOXO dysregulation contribute to infection-induced wasting in *Drosophila*. *Curr. Biol*. 2006; 76:1977–1985. [PubMed: 17055976]
- Fearon KC, Glass DJ, Guttridge DC. Cancer cachexia: mediators, signaling, and metabolic pathways. *Cell Metab*. 2012; 16:153–166. [PubMed: 22795476]
- Fearon K, Arends J, Baracos V. Understanding the mechanisms and treatment options in cancer cachexia. *Nat. Rev. Clin. Oncol*. 2013; 70:90–99. [PubMed: 23207794]
- Figuroa-Clarevega A, Bilder D. Malignant *Drosophila* tumors interrupt insulin signaling to induce cachexia like wasting. *Dev. Cell*. 2015; 33:47–55. this issue. [PubMed: 25850672]
- Gateff E, Schneiderman HA. Developmental capacities of benign and malignant neoplasms of *Drosophila*. *Wilhelm Roux Arch. Entwickl. Mech. Org*. 1974; 176:23–65.
- Géminard C, Rulifson EJ, Leopold P. Remote control of insulin secretion by fat cells in *Drosophila*. *Cell Metab*. 2009; 10:199–207. [PubMed: 19723496]
- Greene JC, Whitworth AJ, Kuo I, Andrews LA, Feany MB, Pallanck LJ. Mitochondrial pathology and apoptotic muscle degener ation in *Drosophila* parkin mutants. *Proc. Natl. Acad. Sci. USA*. 2003; 700:4078–4083. [PubMed: 12642658]
- Grzeschik NA, Paraons LM, Allott ML, Harvey KF, Richardson HE. Lgl, aPKC, and Crumbs regulate the Salvador/Warts/Hippo pathway through two distinct mechanisms. *Curr. Biol*. 2010; 20:573–581. [PubMed: 20362447]
- Halder G, Johnson RL. Hippo signaling: growth control and beyond. *Development*. 2011; 138:9–22. [PubMed: 21138973]
- Han HQ, Zhou X, Mitch WE, Goldberg AL. Myostatin/lactivin pathway antagonism: molecular basis and therapeutic potential. *Int. J. Biochem. Cell Biol*. 2013; 45:2333–2347. [PubMed: 23721881]
- Harvey KF, Hariharan IK. The Hippopathway. *Cold Spring Harb. Perspect. Biol*. 2012; 4:a011288. [PubMed: 22745287]
- Hirabayashi S, Baranski TJ, Cagan RL. Transformed *Drosophila* cells evade diet-mediated insulin resistance through Wingless signaling. *Cell*. 2013; 154:664–675. [PubMed: 23911328]
- Honegger B, Galic M, Kohler K, Wittwer F, Brogiolo W, Hafen E, Stocker H. ImpL2, a putative homolog of vertebrate IGF-binding protein 7, counteracts insulin signaling in *Drosophila* and is essential for starvation resistance. *J. Biol*. 2008; 7:10. [PubMed: 18412985]
- Ikeya T, Galic M, Belawat P, Nairz K, Hafen E. Nutrient-dependent expression of insulin like peptides from neuroendocrine cells in the CNS contributes to growth regulation in *Drosophila*. *Curr. Biol*. 2002; 12:1293–1300. [PubMed: 12176357]

- Ja WW, Carvalho GB, Mak EM, de la Rosa NN, Fang AY, Liang JC, Brummel T, Benzer S. Prandiology of *Drosophila* and the CAFE assay. *Proc. Natl. Acad. Sci. USA.* 2007; 104:8253–8256. [PubMed: 17494737]
- Johnson R, Halder G. The two faces of Hippo: targeting the Hippo pathway for regenerative medicine and cancer treatment. *Nat. Rev. Drug Discov.* 2014; 13:63–79. [PubMed: 24336504]
- Karpowicz P, Perez J, Perrimon N. The Hippo tumor suppressor pathway regulates intestinal stem cell regeneration. *Development.* 2010; 137:4135–4145. [PubMed: 21098564]
- Kir S, White JP, Kleiner S, Kazak L, Cohen P, Baracos VE, Spiegelman BM. Tumour-derived PTH-related protein triggers adipose tissue browning and cancer cachexia. *Nature.* 2014; 513:100–104. [PubMed: 25043053]
- Menéndez J, Perez Garijo A, Calleja M, Morata G. A tumor-suppressing mechanism In *Drosophila* Involving cell competition and the Hippo pathway. *Proc. Natl. Acad. Sci. USA.* 2010; 107:14651–14656. [PubMed: 20679206]
- Murali T, Pacifico S, Yu J, Guest S, Roberts GG III, Finley RL Jr. DrolD 2011: a comprehensive, Integrated resource for protein, transcription factor, RNA and gene Interactions for *Drosophila*. *Nucleic Acids Res.* 2011; 39:D736–D743. [PubMed: 21036869]
- O'Brien LE, Sollman SS, Li X, Biider D. Altered modes of stem cell division drive adaptive Intestinal growth. *Cell.* 2011; 147:603–614. [PubMed: 22036568]
- Oh H, Irvine KD. In vivo analysis of Yorkle phosphorylation sites. *Oncogene.* 2009; 28:1916–1927. [PubMed: 19330023]
- Pan D. The Hippo signaling pathway In development and cancer. *Dev. Cell.* 2010; 19:491–505. [PubMed: 20951342]
- Penna F, Minero VG, Costamagna D, Bonelli G, Baccino FM, Costelli P. Anti-cytokine strategies for the treatment of cancer-related anorexia and cachexia. *Expert Opin. Biol. Ther.* 2010; 10:1241–1250. [PubMed: 20594117]
- Planté-Bordeneuve V, Said G. Familial amyloid polyneuropathy. *Lancet Neurol.* 2011; 10:1086–1097. [PubMed: 22094129]
- Puig O, Tjlan R. Transcriptional feedback control of Insulin receptor by dFOXO/FOXO1. *Genes Dev.* 2005; 19:2435–2446. [PubMed: 16230533]
- Ren F, Wang B, Yue T, Yun EY, Ip YT, Jiang J. Hippo signaling regulates *Drosophila* Intestine stem cell proliferation through multiple pathways. *Proc. Natl. Acad. Sci. USA.* 2010; 107:21064–21069. [PubMed: 21078993]
- Rommel C, Bodine SC, Clarke BA, Rossman R, Nunez L, Stitt TN, Yancopoulos GD, Glass DJ. Mediation of IGF-1-Induced skeletal myotube hypertrophy by PI(3)K/Akt/mTOR and P(3)K/Akt/GSK3 pathways. *Nat. Cell Biol.* 2001; 3:1009–1013. [PubMed: 11715022]
- Sandri M, Sandri C, Giibert A, Skurk C, Calabria E, Picard A, Walsh K, Schiaffino S, Lecker SH, Goldberg AL. Foxo transcription factors Induce the atrophy-related ubiquitin ligase atrogin-1 and cause skeletal muscle atrophy. *Cell.* 2004; 117:399–412. [PubMed: 15109499]
- Shaw RL, Kohlmaler A, Polesello C, Veelken C, Edgar BA, Tapon N. The Hippo pathway regulates Intestinal stem cell proliferation during *Drosophila* adult midgut regeneration. *Development.* 2010; 137:4147–4158. [PubMed: 21068063]
- Sloth Andersen A, Hertz Hansen P, Schaffer L, Kristensen C. A new secreted insect protein belonging to the immunoglobulin superfamily binds insulin and related peptides and inhibits their activities. *J. Biol. Chem.* 2000; 275:16948–16953. [PubMed: 10748036]
- Song W, Ren D, Li W, Jiang L, Cho KW, Huang P, Fan C, Song Y, Liu Y, Rul L. SH2B regulation of growth, metabolism, and longevity In both Insects and mammals. *Cell Metab.* 2010; 11:427–437. [PubMed: 20417156]
- Song W, Veenstra JA, Perrimon N. Control of lipid metabolism by tachykinin in *Drosophila*. *Cell Rep.* 2014; 9:40–47. [PubMed: 25263556]
- Staley BK, Irvine KD. Hippo signaling In *Drosophila*: recent advances and Insights. *Dev. Dyn.* 2012; 241:3–15. [PubMed: 22174083]
- Subramanian A, Tamayo P, Mootha VK, Mukherjee S, Ebert BL, Gillette MA, Paulovich A, Pomeroy SL, Golub TR, Lander ES, Mesirov JP. Gene set enrichment analysis: a knowledge based

- approach for Interpreting genome-wide expression profiles. *Proc. Natl. Acad. Sci. USA.* 2005; 102:15545–15550. [PubMed: 16199517]
- Teleman AA, Chen YW, Cohen SM. 4E BP functions as a metabolic brake used under stress conditions but not during normal growth. *Genes Dev.* 2005; 19:1844–1848. [PubMed: 16103212]
- Tisdale MJ. Biology of cachexia. *J. Natl. Cancer Inst.* 1997; 89:1763–1773. [PubMed: 9392617]
- Tisdale MJ. Mechanisms of cancer cachexia. *Physiol. Rev.* 2009; 89:381–410.
- Trapnell C, Pachter L, Salzberg SL. TopHat: discovering splice junctions with RNA-seq. *Bioinformatics.* 2009; 25:1105–1111.
- Trapnell C, Roberts A, Goff L, Pertea G, Kim D, Kelley DR, Pimentel H, Salzberg SL, Rinn JL, Pachter L. Differential gene and transcript expression analysis of RNA-seq experiments with TopHat and cufflinks. *Nat. Protoc.* 2012; 7:562–578. [PubMed: 22383036]
- Vander Heiden MG, Cantley LC, Thompson CB. Understanding the Warburg effect: the metabolic requirements of cell proliferation. *Science.* 2009; 324:1029–1033. [PubMed: 19460998]
- Vander Heiden MG, Lunt SY, Dayton TL, Fiske BP, Israelsen WJ, Mattaini KR, Vokes NI, Stephanopoulos G, Cantley LC, Metallo CM, Locasale JW. Metabolic pathway alterations that support cell proliferation. *Cold Spring Harb. Symp. Quant. Biol.* 2011; 76:325–334. [PubMed: 22262476]
- Warburg O. On the origin of cancer cells. *Science.* 1956; 123:309–314. [PubMed: 13298683]
- Yang X, Xu T. Molecular mechanism of size control in development and human diseases. *Cell Res.* 2011; 21:715–729. [PubMed: 21483452]
- Ye X, Deng Y, Lal ZC. Akt is negatively regulated by Hippo signaling for growth inhibition in *Drosophila*. *Dev. Biol.* 2012; 369:115–123. [PubMed: 22732571]
- Yuan M, Brechtkopf SB, Yang X, Asara JM. A positive/negative ion switching, targeted mass spectrometry based metabolomics platform for bodily fluids, cells, and fresh and fixed tissue. *Nat. Protoc.* 2012; 7:872–881. [PubMed: 22498707]
- Zhang W, Thompson BJ, Hietakangas V, Cohen SM. MAPK/ERK signaling regulates insulin sensitivity to control glucose metabolism in *Drosophila*. *PLoS Genet.* 2011; 7:e1002429. [PubMed: 22242005]
- Zinke I, Kirchner C, Chao LC, Tetzlaff MT, Pankratz MJ. Suppression of food intake and growth by amino acids in *Drosophila*: the role of pumless, a fat body expressed gene with homology to vertebrate glycine cleavage system. *Development.* 1999; 126:5275–5284. [PubMed: 10556053]

Highlights

- Localized Yki-induced overproliferation causes systemic organ wasting in *Drosophila*
- The secreted insulin/IGF antagonist ImpL2 is a mediator of systemic organ wasting
- ImpL2, secreted from overproliferating tissue, reduces systemic insulin/IGF signaling
- Overproliferating tissue evades wasting via local elevation of insulin/IGF signaling

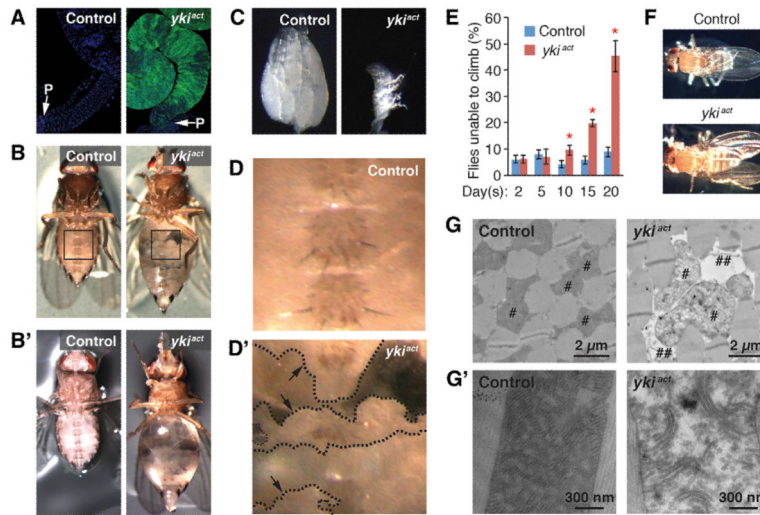


Figure 1. Degeneration of Ovary, Fat Body, and Muscle in *esg^{ts}>yki^{act}* Flies

(A) Midgut images. GFP is driven by *esg^{ts}* (*esg-GAL4*, *tub-GAL80^{ts}*, *UAS-GFP/+*). The arrows indicate the posterior (P) end of the midgut.

(B and B') Fly images. Transgenes were induced for 6 days (B) and 12 days (B') with *esg^{ts}*.

(C) Ovary images. Transgenes were induced for 8 days.

(D and D') Magnified views of the insets in (B). The dashed lines and arrows indicate the boundary of the fat body.

(E) Quantification of climbing defects (mean \pm SEMs). * $p < 0.05$, Student's *t* test.

(F) Downturned wing phenotype in *esg^{ts}>yki^{act}* flies.

(G) Electron microscopic images of the transverse section of indirect flight muscles. #, mitochondria; ##, empty spaces.

(G') Images of mitochondrion. In all muscle experiments, transgenes were induced for 20 days in male flies unless otherwise indicated. The genotype of control is *esg-GAL4*, *tub-GAL80^{ts}*, *UAS-GFP/+* and *yki^{act}* is *esg-GAL4*, *tub-GAL80^{ts}*, *UAS-GFP/+*; *UAS-yki^{act}/+*.

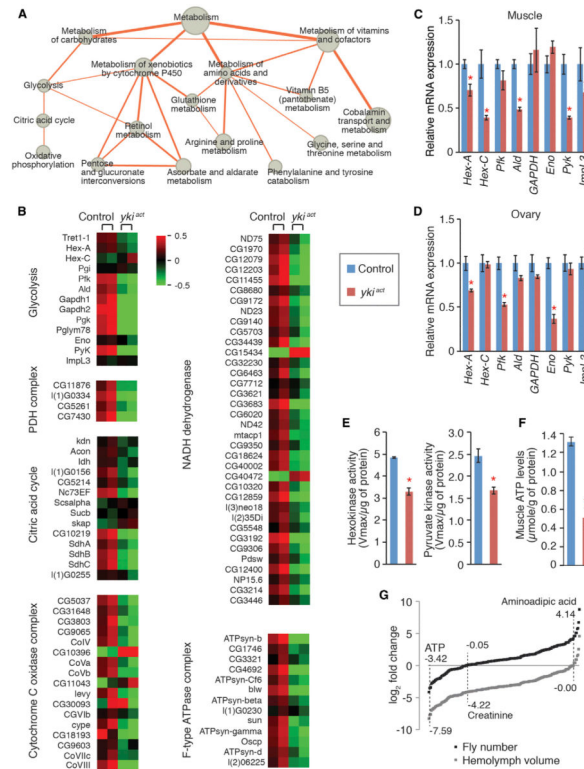


Figure 2. Repression of Energy Metabolism in *esg^{ts}>yki^{act}* Muscles

(A) Network presentation of gene list enrichment analysis results focusing on metabolism. All presented metabolic processes are identified to be significantly downregulated in muscles of *esg^{ts}>yki^{act}* flies (Tables S2 and S3). Node size indicates enrichment ($-\log_{100}$ p value), and edge thickness represents the number of common genes between two gene sets. The citric acid cycle and pyruvate metabolism ($p = 0.0253$, GSEA) and oxidative phosphorylation ($p = 0.000$, GSEA) are identified by GSEA analysis (Subramanian et al., 2005).

(B) Representative downregulated processes and complexes involved in energy metabolism. Heat map signal indicates \log_2 fold-change values relative to the mean expression level within the group. Red signal denotes higher expression and green signal denotes lower expression relative to the mean expression level within the group. Related GSEA plots are shown in Figure S1.

(C and D) Relative mRNA expression of glycolytic enzyme in muscle (C) and ovaries (D). Measurements shown are mean \pm SDs.

(E) Activities of Hexokinase (left) and Pyruvate kinase (right) in muscle at 8 days of induction (mean \pm SEMs).

(F) ATP levels in muscle at 20 days of transgene induction.

(G) Metabolomic analysis of hemolymph metabolites. The metabolite counts are normalized to fly number (black) or extracted hemolymph volume (gray). \log_2 fold-change values of the metabolites in hemolymph of *esg^{ts}>yki^{act}* flies relative to control are presented. Reduced 55 metabolites in hemolymph of *esg^{ts}>yki^{act}* flies are shown in Figure S2. * $p < 0.05$ (Student's t test) compared to control. Genotypes are as shown in Figure 1.

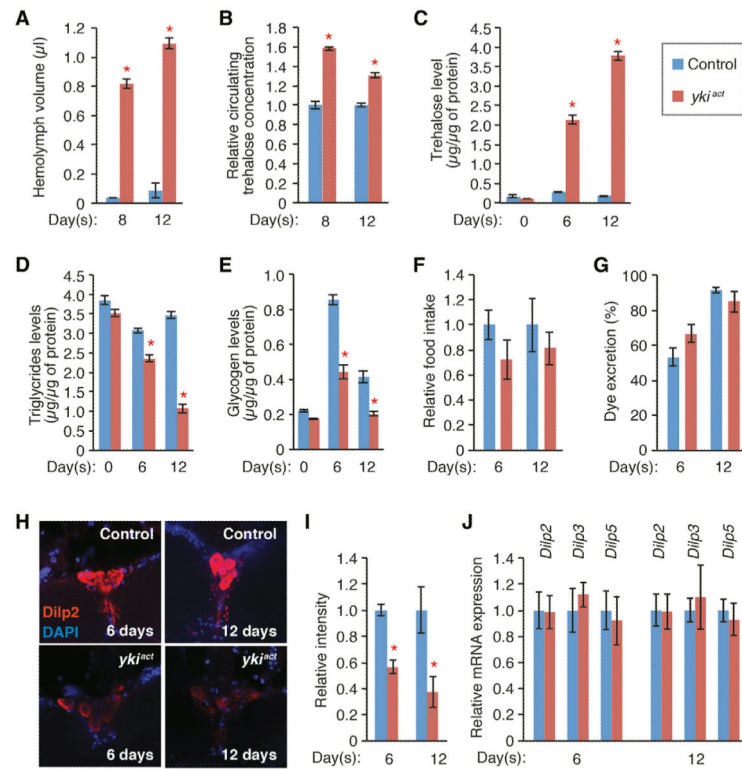


Figure 3. *esg^{TS}>ykt^{act}* Causes Hyperglycemia and Depletion of Triglycerides and Glycogen

(A) Volumes of extractable hemolymph per fly after 8 and 12 days of induction with *esg^{TS}*.

(B) Relative concentration of circulating trehalose normalized to control at 8 and 12 days of induction.

(C) Trehalose levels in whole flies normalized to extracted protein amounts at different induction times.

(D) Triglyceride levels in whole flies. Triglyceride levels were normalized to protein amounts.

(E) Glycogen levels in whole flies. Glycogen levels were normalized to protein amounts.

(F) Food intake measured by CAFE assay (Demontis and Perrimon, 2010; Ja et al., 2007) after 6 and 12 days of transgene induction with *esg^{TS}*. Values relative to controls are presented.

(G) Food excretion rate. Transgenes are induced for 6 and 12 days. The percentages of excreted dye amount to total intake are shown.

(H) Dilp2 staining in the IPCs in the brain. Images are captured with the same confocal setting.

(I) Quantification of Dilp2 signal intensity in IPCs. Dilp2 signals are normalized to background signals, and values relative to controls are presented.

(J) mRNA levels in the heads measured by qPCR. The results shown in (A)–(E) are mean \pm SEMs. The values in (F), (G), (I), and (J) are mean \pm SDs. *p < 0.05 (Student's t test) compared to control. Genotypes are as shown in Figure 1.

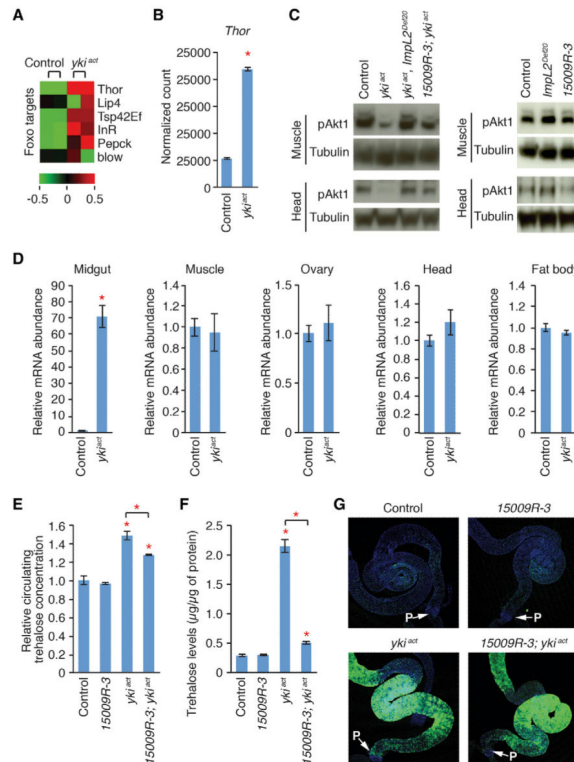


Figure 4. Depletion of *ImpL2* from *esg^{ts}*>*yki^{act}* Midgut Rescues Systemic Reduction of Insulin/IGF Signaling and Hyperglycemia

(A) Heat map showing expression of the Foxo target gene set. Foxo target genes are annotated from Droid (Murali et al., 2011).

(B) Normalized expression levels of *Thor* (human 4E-BP ortholog). The values shown are mean \pm SEMs. The asterisk denotes statistically significant difference from control (adjusted $p = 1.239 \times 10^{-87}$; p values are adjusted with the Benjamini-Hochberg procedure, which controls the false discovery rate; Benjamini and Hochberg, 1995).

(C) Akt1 phosphorylation in muscle and head at 8 days of induction.

(D) Relative expression levels of *ImpL2* mRNA in the midgut, muscle, ovary, head, and fat body. The active form of *yki* (*yki^{act}*) was expressed in the midgut with *esg^{ts}* for 6 days. The values are mean \pm SDs. * $p < 0.05$, unpaired Student's *t* test.

(E) Circulating trehalose concentrations at 8 days of induction.

(F) Trehalose levels in the whole-body void at 6 days of induction. The measurements are normalized to total protein amounts.

The results shown in (E) and (F) are mean \pm SEMs. * $p < 0.05$ (Student's *t* test) compared to control other than when indicated by a bracket.

(G) Midgut morphology. GFP is driven by *esg^{ts}* and *UAS-GFP*. Nuclei are marked with 4',6-diamidino-2-phenylindole (DAPI) (blue). The arrows indicate the posterior end of the midgut. The genotype of control is *esg-GAL4, tub-GAL80^{ts}, UAS-GFP/+*, *yki^{act}* is *esg-GAL4, tub-GAL80^{ts}, UAS-GFP/+*; *UAS-yki^{act}/+*, *yki^{act}, ImpL2^{Def20}* is *esg-GAL4, tub-GAL80^{ts}, UAS-GFP/+*; *UAS-yki^{act}, ImpL2^{Def20}/ImpL2^{Def20}*, *15009R-3* is *esg-GAL4, tub-GAL80^{ts}, UAS-GFP/15009R-3* (*UAS-ImpL2* RNAi from the National Institute of Genetics,

Japan), *15009R-3*; *yki^{act}* is *esg-GAL4*, *tub-GAL80^{ts}*, *UAS-GFP/15009R-3*; *UAS-yki^{act/+}*, and *ImpL2^{Def20}* is *esg-GAL4*, *tub-GAL80^{ts}*, *UAS-GFP/+*; *ImpL2^{Def20}/ImpL2^{Def20}*.

Author Manuscript

Author Manuscript

Author Manuscript

Author Manuscript

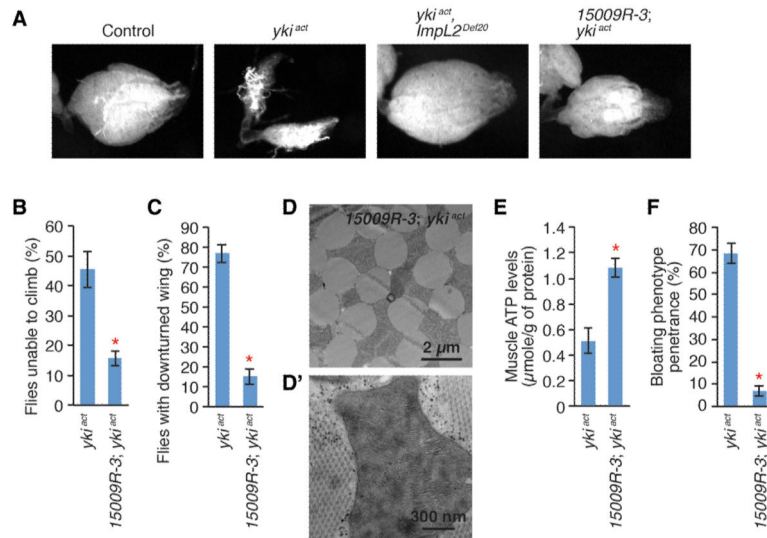


Figure 5. Depletion of *Impl2* with *esg^{ts}* Rescues Degeneration of Ovaries and Muscle Associated with *esg^{ts}>yki^{act}*

(A) Images of ovaries from the indicated geno types. Transgenes are induced for 8 days with *esg^{ts}*

(B) Quantification of climbing defect.

(C) Penetrance of downturned wing phenotype.

(D) Electron microscopic image of transverse section of indirect flight muscles.

(D) Image of mitochondrion.

(E) Muscle ATP levels normalized to protein levels. In all muscle experiments, transgenes are induced for 20 days in male flies.

(F) Penetrance of the bloating syndrome at 8 days of transgene induction. Either control (*esg^{ts}*) or expression of *15009R-3* alone with *esg^{ts}* is not associated with the bloating syndrome phenotype.

All quantifications shown are mean ± SEMs. * $p < 0.05$, Student's t test compared to *yki^{act}*. Genotypes are as shown in Figure 4.

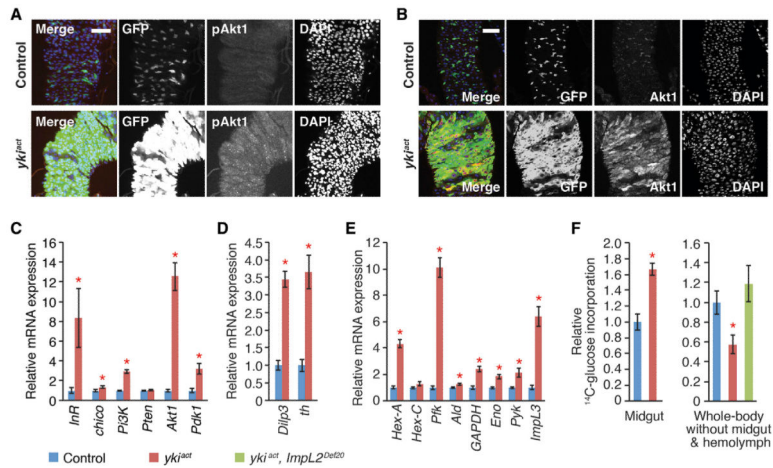


Figure 6. Upregulation of Insulin/IGF Signaling in *esg^{ts}>yki^{act}* Midguts

(A and B) Both phosphorylation of Akt1 (pAkt1; red in merge; A) and expression of Akt1 (red in merge; B) are increased in *esg^{ts}>yki^{act}* midguts. Nuclear staining is shown with DAPI (blue in merge). The scale bars represent 50 μ m. We characterized anti-Aki and anti-pAkt antibodies in the midgut (Figure S7).

(C) Relative mRNA expression of insulin/IGF pathway components in the midgut measured by qPCR at 6 days of induction.

(D) Relative expression of *dilp3* mRNA in *esg^{ts}>yki^{ts}* midgut at 6 days of induction. *thread* (*th*) is a known transcriptional target of *yki*.

(E) Relative mRNA abundance of glycolytic enzymes in the midgut of *esg^{ts}>yki^{act}* flies at 8 days of induction.

(F) [14 C]glucose incorporation in the midgut (left) and whole-body void of midgut and hemolymph (right).

All qPCR values are mean \pm SDs, and other measurements are mean \pm SEMs. Transgenes are induced with *esg^{ts}* by shifting to the nonpermissive temperature (29°C). * $p < 0.05$, Student's t test compared to control. Genotypes are as shown in Figure 4.

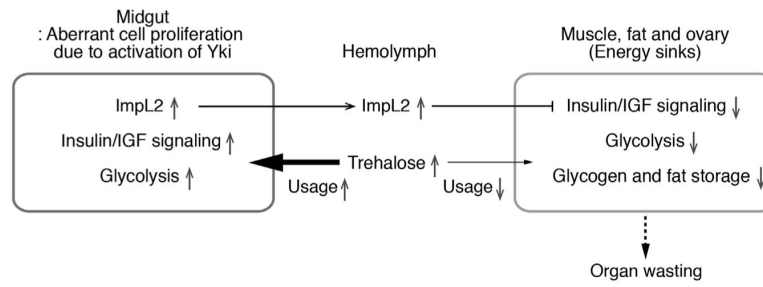


Figure 7.
Model of the Tissue Autonomous and Systemic Changes Caused by Aberrant Activation of Yki in ISCs